ENERGY LEVEL EFFECTS ON DEFORMATION MECHANISM IN MICRO-SCALE LASER PEEN FORMING

Youneng Wang, Yajun Fan, Sinisa Vukelic, Y. Lawrence Yao
Department of Mechanical Engineering
Columbia University, New York, NY 10027

KEYWORDS

Laser micro-scale peen forming, X-ray micro-diffraction, forming mechanism

ABSTRACT

Laser micro-scale peen forming has recently received a great deal of attention as a viable laser processing technology as it not only imparts desirable residual stress for the improvement of fatigue life of the material, but can also precisely control part deformation. In the present study, the effect of energy level on deformation mechanism in laser micro-scale peen forming was investigated by both numerical and experimental methods. Deformation curvatures and residual stress distributions of both sides of the specimen are characterized by X-ray micro-diffraction and compared with the results obtained from FEM simulation. The forming mechanism for convex and concave bending phenomena was explained in terms of the resulting pressure, compressive stress distribution, and plastic strain. Differences in residual stress distributions were also investigated as a function of forming mechanism

INTRODUCTION

Laser forming, usually indicating laser thermal forming, is a flexible rapid prototyping and low-volume manufacturing process, which uses laser-induced thermal distortion to shape sheet metal parts without tooling or external forces. It is well understood both from theoretical and experimental investigations because of its technological advantages as compared to the conventional forming technologies, including design flexibility, production of complex shapes, forming of thick plates, and possibility of rapid prototyping (Vollertsen, 1994). One difficulty, however, is maintaining desirable material properties of metallic parts. This is due to thermal effects that result in undesirable microstructure changes including recrystallization and phase transformation even without the presence of melting. Also, laser thermal forming may melt or burn the surface and even result in small cracks on the surface.

Laser peen forming (LPF) (also known as laser shock forming), developed from laser shock peening technology (Clauer and Holbrook, 1981), is a non-thermal laser forming method achieved through the use of laser energy to modify the curvature of the target. It has the advantages of non-contact, tool-less, high efficiency and precision. Also, its non-thermal nature makes it possible to maintain material properties or even improve them by inducing compressive stress over the target surface. This is desirable as it is important in industry for shaped metal parts to resist cracks due to corrosion and fatigue. In addition, such a compressive stress will generate a strain of the top layer of metal and produce a curvature (Hackel, 2002). Hackel et al. (2002) demonstrate that the part can be precisely contoured over its large area by systematically applying impulses inducing local stresses. Zhou et al. (2002) show the potential of laser peen forming for becoming a flexible manufacturing process with desirable properties as well as the potential for rapid prototyping. They provide insight on deformation mechanisms, mechanical response and failure behavior for materials under this process. Despite the recent advances, the process has still not been fully characterized due to its complex underlying mechanisms for deformation.

In the last ten years, miniaturization technologies have revolutionized product design and lead to many innovative applications requiring new techniques for the manufacture of complex miniaturized devices. This serves as the driving fore for the investigation of micro-scale laser peen forming (μLPF) as a potential method of micro-forming. There currently exists a great deal of work demonstrating that micro-scale laser shock peening (Chen et al., 2004), produces local compressive stress near the surface, thus improving macro-scale material properties. Therefore, it is possible to employ μLPF to machine complex miniaturized devices as well as improve the fatigue life of the material.

In this paper, micro-scale laser peen forming is studied using both numerical and experimental methods. The effects of different laser energies on deformation mechanism were investigated experimentally and a corresponding simulation model was then validated based on the experimental results. The sample curvatures before and after laser micro-scale peen forming were measured using a profilometer to find the net bending effect of the process. Also, both residual stress distributions on the top and bottom surfaces were measured using X-ray micro-diffraction. In addition, phenomena about concave and convex bending which result in different patterns of residual stress distribution along the sample's surface were explored. The numerical simulation verified from the experimental results can then be used to predict the deformation and understand the forming mechanism. Hence, the presented work laid some foundation for understanding the process of micro-scale laser peen forming.

PROCESS OF MICRO-SCALE PEEN FORMING AND EXPERIMENT CONDITIONS

Principles of micro-scale laser peen forming

Developed from laser micro-scale shock peening technology, micro-scale laser peen forming may be employed to precisely shape structural components with micro-scale resolution. Both micro-scale laser shock peening (μLSP) and peen forming apply a short intense laser pulse using a micron-sized beam to treat the metallic target surface and compressive stress is then imparted on the treated surface with micron-level spatial resolution without introducing any thermal effects. For μLSP, the target is placed on a rigid substrate in order to prevent any movement of the bottom surface. Thus, the resulting compressive residual stress will be maximized on the surface and plastic strain is mainly imparted on the top surface. However, the bottom of target is not restricted for μLPF and two ends are clamped by two metal sheets. Typically, the target thickness is much thinner than that of μLSP. Hence, plastic strain may be induced in both sides and the resulting compressive stress on the treated surface will cause that surface to expand thus plastically curving the metal. The curved shape may be convex or concave depending upon process parameters. In addition, the surfaces of both sides may be left in a compressive state of stress which is highly desirable for fatigue and corrosion resistance. Therefore, the process of μLPF is relatively complex compared with μLSP since it involves both local and global plastic deformation.

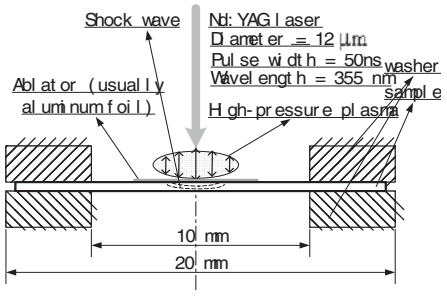

FIG. 1 SAMPLE GEOMETRY AND LASER SHOCK FORMING CONDITION

Experiment conditions and sample preparation

A frequency tripled Q-switched Nd:YAG laser ($\lambda = 355\,nm$) in TEM_{00} mode was used in μLPF and the parameters of pulse duration, wavelength and beam diameter are shown in Fig. 1. A line of μLSP shocks was created on the sample surface with a 25μm spacing. Pulse energies, 202 and 280μJ, corresponding to laser intensities of 3.57 and 4.95GW/cm^2, respectively, were applied. A thin layer of high vacuum grease (about 10 microns thick) was spread evenly on the sample surface, and a 16μm thick polycrystalline aluminum foil, chosen for its relatively low threshold of vaporization, was tightly pressed onto the grease. The

sample was placed in a shallow container filled with distilled water around 1 mm above the sample's top surface. The induced deformation is due to shock pressure and not due to thermal effects since only the coating is vaporized during the process.

The sample of copper foils with 100μm thickness and 3mm width have been chosen, due to their strong (001) texture, and may be treated as a single crystal in micro-diffraction measurements. Because copper foils were made by a rolling process, the samples were heat treated to release stress at a temperature of 150°C for one hour. After heat treatment, the texture was measured again by using the conventional X-ray and was found that the stress relief process has almost no effect on texture. The samples were cut to the dimension of 20mm×3mm by using a wire EDM and mounted to holders as shown in Fig.1 ensuring the specimens are as flat as possible. Before the shocking process, pre-bending is measured using a Mitutoyo SJ-201P profilometer as shown in Fig. 2 and the samples with a pre-bending less than 8μm were chosen for treatment so as to minimize the pre-bending effects.

POST-PEEN FORMING MATERIAL CHARACTERIZATION

Curvature measurement by using profilometer

After laser peen forming, the samples' profile was measured using Surftest SJ-201P of Mitutoyo. This surftester's measuring range is 350μm with the resolution 0.4μm. The measuring force is 4mN, which assures the detector has no bending effect on the samples while measuring. The measured results are shown in Fig. 2. It can be seen that the bend is downward 8μm for the 100μm sample with laser intensity 3.57GW/cm^2; that is, concave surface is left upon curving. For 100μm sample with laser intensity 4.95GW/cm^2, the bend is upward 10μm; that is, convex. Also, from Fig. 2, it can be calculated that the bending angle is about 0.11°, 0.14° for these two energy levels, respectively. Thus micro-scale laser peen forming is capable of producing plastic deformation at micro-scale resolution.

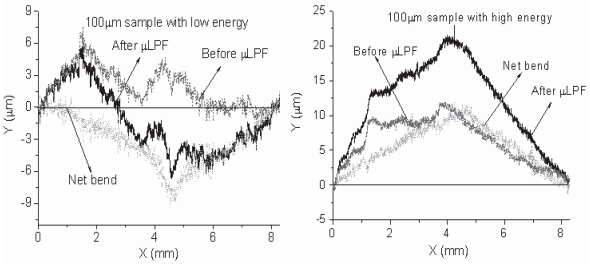

FIG. 2 CURVATURE MEASUREMENT BEFORE AND AFTER PEENFORMING: A)3.57GW/CM^2 INTENSITY; B) 4.95GW/CM^2 INTENSITY

Residual stress distribution by X-ray micro-diffraction

X-ray beams from synchrotron radiation sources (from beamline X20A at National Synchrotron Light Source at Brookhaven National Lab) were used in this study as the extreme intensities allow a short sampling time and further, the X-ray can be focused by a tapered glass capillary to spot sizes as small as 3 microns. Complete details of the X-ray micro-diffraction experiment and the corresponding evaluation method of sub-profile analysis can be found in Chen, et al. (2004). Because the copper samples used has a very strong texture in the (001) orientation, (002) reflections are chosen for X-ray diffraction measurement since the diffraction structure factor for (001) is zero and the reflections are absent (Cullity, 1978). In order to spatially resolve the residual stress induced by μLPF, measurements were made on both top and bottom surfaces across the peened line. The spacing between adjacent measurement points is 10μm and the corresponding X-ray diffraction profile at each position is recorded and repeated for each scan line. After obtaining the X-ray diffraction profiles at different positions in the peened region, the lateral residual stress on the surface can be estimated using the sub-profile method of Chen, et al. (2004). The spatial distribution across the peened region plotted as in Fig. 3. It can be seen from Fig. 3(a) that a compressive residual stress is generated near the center of the peened region and is bordered by a region of tensile stress on both sides for the bottom surface under 3.57GW/cm^2 laser intensity. And there is a tensile residual stress near the center which is bordered by a region of compressive stress on the top surface. For 4.95GW/cm^2 laser energy, a compressive residual stress is

generated on both bottom and top surfaces. Although the laser spot size is only 12μm, the high shock pressure in μLPF can generate significant compressive residual stresses over a much larger region, up of to 200μm. For the 4.95GW/cm^2 condition, the induced compressive stress is also larger than that of 3.57GW/cm^2. The compressive stress is estimated to have a maximum value of –150MPa near the center and cover a region 120μm from the center for the 4.95GW/cm^2 laser intensity. It can be seen that compressive residual stresses are induced in both sides for the convex bending where the top side is tensile and the bottom side is compressive for concave bending.

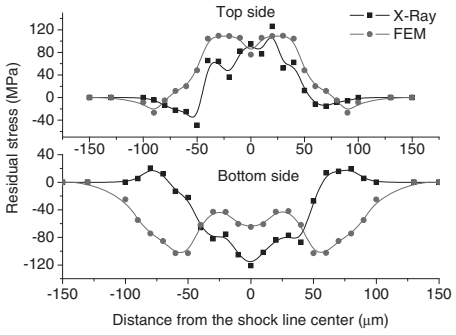

(a)

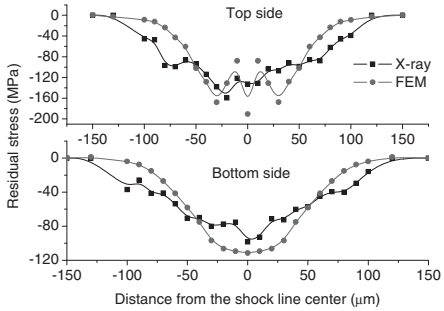

(b)

FIG. 3 RESIDUAL STRESS BY X-RAY MICRO-DIFFRACTION AND SIMULATION FOR 100μM SAMPLE: A) 3.57GW/CM^2 INTENSITY; B)4.95GW/CM^2 INTENSITY.

FEM SIMULATION

Shock pressure, hardening and strain rate effects

For this numerical simulation, the laser forming process is modeled as purely mechanical. The analytical shock model in this paper follows Fabbro's model (1990), which assumes that the laser irradiation is uniform and shock propagation in the confining medium is one-dimensional. The spatially non-uniform shock pressure may be modeled as $P(r,t) = P(t)\exp(-r^2/2r_0^{\,2})$, where r is the radial distance from the center of the laser beam, and r_0 the radius of laser beam, which is 6μm in this paper.

In LSP, the target is subjected to a very strong shock pressure (>1 GPa), a very short interaction time (<100 ns), and very high strain rate (>100,000 s^{-1}). The increased strain rate has a much greater effect on the material flow stress in LSP than static loading, which in turn, influences the deformation of the material. The total strain rate during laser forming can be decomposed into $\dot{\varepsilon}_{ij} = \dot{\varepsilon}^e_{ij} + \dot{\varepsilon}^p_{ij}$, where $\dot{\varepsilon}_{ij}$, $\dot{\varepsilon}^e_{ij}$ and $\dot{\varepsilon}^p_{ij}$ represent total strain rate, elastic strain rate, and plastic strain rate. The relation between strain ε_{ij} and stress σ_{ij} under plastic deformation can be written as

$$d\varepsilon_{ij} \approx d\varepsilon^p_{ij} = (d\lambda)\frac{df}{d\sigma_{ij}} \qquad (1)$$

since $\dot{\varepsilon}^e_{ij}$ is much smaller than $\dot{\varepsilon}^p_{ij}$. Where f is the flow potential and $d\lambda$ is the rate of change of time, dt, whose value is determined by the requirement to satisfy the consistency condition $f = 0$, for plastic flow of rate-independent model. When Von Mises criterion is applied for f, the above equation takes the following form for $d\varepsilon_{11}$:

$$d\varepsilon^p_{11} = d\lambda\frac{\partial}{\partial\sigma_{11}}\left\{\frac{1}{6}\left[(\sigma_{11}-\sigma_{22})^2+(\sigma_{11}-\sigma_{22})^2+(\sigma_{11}-\sigma_{22})^2\right]+\sigma^2_{12}+\sigma^2_{13}+\sigma^2_{23}\right\}$$
$$= (d\lambda)S_{11}$$

where S_{ij} is the deviatoric part of stress.

In the numerical simulation, the isotropic hardening is accounted for by a Johnson-Cook plasticity law which takes both strain and strain rate effects into consideration. Based on the Johnson-Cook model, the yield strength is written as:

$$Y = Y_0[1 + C\ln\frac{\dot{\varepsilon}}{\dot{\varepsilon}_0}][1 + B\varepsilon]^n\left(1 - \frac{T - T_0}{T_m - T_0}\right) \qquad (2)$$

where C is the logarithmic rate sensitivity, ε is strain, $\dot{\varepsilon}$ is strain rate, B and n are material parameters describing work hardening effect. In this paper, the temperature effect is negligible since there is no thermal effect in LSP.

Simulation conditions

In the simulation, a two-dimensional deformation state of plane strain condition was assumed. This is reasonable since μLSP results in a two-dimensional deformation if shocking the sample under the condition as described in Section 2 (Chen, et al., 2004). A length of 10mm is computed and bias mesh in lateral direction is applied with the finest mesh in the middle as small as 2.3μm, which is much smaller than the laser beam of 12μm. The mesh in the depth direction is constant with the size of 2μm. CPE4R elements were employed in the analysis. Also, the two ends of the sample are fixed in the simulation and the bottom and top sides are free.

The finite element solvers, ABAQUS/Explicit and ABAQUS/Standard, were combined to perform the simulation. These two solvers accomplish different calculations during this simulation. The simulation is divided into two steps: i) a high dynamic laser shock loading with the explicit version without mass scaling; ii) static unloading corresponding to the relaxation process with the implicit version. After the ABAQUS/Explicit analysis finishes, the information including the stress, strain and displacement data was exported to the ABAQUS/Standard analysis. The ABAQUS/Explicit module is a non-linear, explicit, time integration finite element code, which is especially well suited for solving high speed, short duration, highly dynamic events that require many small time step increments to obtain a high resolution solution. One important issue about the modeling is the balance between a short time for dynamic shock-solid interaction (2~3 times of the laser pulse duration) and a much longer relaxation time (up to 1 second) to reach a stabilized mechanical state.

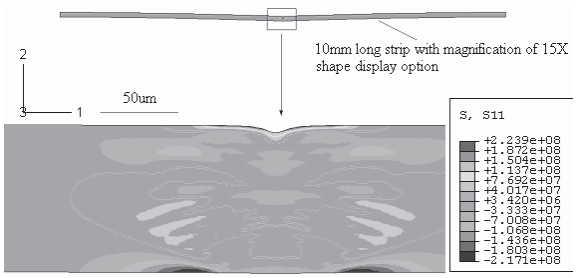

(a)

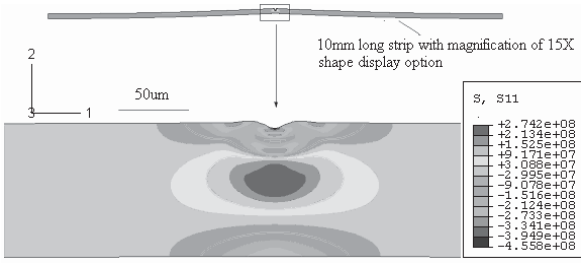

(b)

FIG. 4 RESIDUAL STRESS CONTOUR AFTER PEEN FORMING BY SIMULATION: A) 3.57GW/CM^2 INTENSITY; B) 4.95GW/CM^2 INTENSITY

Simulation model validation

In Fig. 4(a), the calculated residual stress field near the laser shocked region of the 100μm sample with 3.57GW/cm^2 is shown. The residual stress contour of the whole computed length indicates that the bend is downward. This trend is the same as that of the experimental result as shown in Fig. 2(a). The simulation result for the 100μm sample with high energy is shown in Fig. 4(b), whose bending direction is consistent with the experiment result from the profilometer (Fig. 2(b)). For the residual stress distribution, we can find from Fig. 4 that the simulation model gives the almost same patterns as the experiment results; that is, the top side is mainly tensile stress, while the bottom side is compressive for the 3.57GW/cm^2 case, and both sides are compressive for the 4.95GW/cm^2 case. In order to compare the simulation results of residual stress with the experimental results, the corresponding residual stress of the simulation at each point was obtained by averaging over the effective penetration depth of X-ray micro-diffraction. Choosing the depth of 95 percent of the total diffracted intensity (Cullity, 1978):

$$x = \frac{3 \times \sin\theta_0}{2\mu} \qquad (3)$$

where θ_0 is the ideal Bragg angle, μ is the linear absorption coefficient and the effective depth is approximately 15μm for the copper. In this surface layer of depth 15 μm, the averaged stresses at each point with respect to X-ray measurement points were obtained and are shown in Fig. 3. It can be seen that the simulation results show similar patterns and generally agree with the experimental results. Fig. 5 shows the comparison of the curvature

after peen forming for the simulation and experiment. The simulated profiles agree well with the experimental results from profilometer as well as the overall deformation depth. These general agreements for residual stress distribution and deformation are indicative of the model's validity. Thus, the model can be used to predict the response to μLPF for different process parameters.

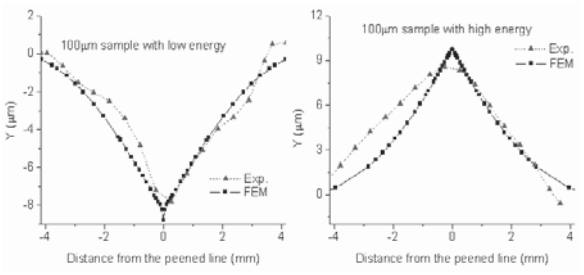

FIG. 5 CURVATURE COMPARISON OF FEM AND EXPERIMENTAL RESULTS: A)3.57GW/CM^2 INTENSITY; B) 4.95GW/CM^2 LASER INTENSITY

FURTHER INVESTIGATION OF DISTINCTIVE FORMING MECHANISMS

Physical explanation

Laser micro-scale peen forming is a purely mechanical process. It imparts compressive stress through a compressive shock wave on the surface of the metal to deform the target. When the laser pulse ablates the coating, the material area beneath the ablating coating undergoes local plastic deformation, which can result in either concave or convex curvature as shown in Section 3.1. It is of great interest to understand this phenomenon since it is related not only to final deformation shape but also to residual stress distribution.

It can be imagined that the specimen will bend downward first under the downward loading if thickness is thinner enough and this downward trend continues during relaxing until opposite sources overcome this downward inertia. In addition, the stress distribution in lateral direction is tensile on the bottom side to balance the top's compressive stress so that this downward bending reinforces plastic deformation on bottom side since it stretches the bottom. After the inertia disappears, there is a reverse bending followed. This phenomenon may be determined by three sources, such as the downward loading (inertia after the loading), bending moment and induced compressive stress, which function together to determine the bending. During the loading, the pressure resulted from laser ablation is the dominant source, which consequently induces the other two sources. Since the loading direction is downward and the sample is free on the bottom side, the bend will be downward in the loading stage. However, the induced compressive stress on top surface will cause that surface to expand, which exerts bulging to the specimen. In addition, the bending angle results in an opposite bending moment and exerts bulging to the specimen, too.

During unloading, the inertia makes the specimen bend downward continuously until the other two sources exceed the effect of the inertia. Then, the forming direction of the specimen is reversed when compressive stress becomes dominant. Thus, the phenomenon that the concave or convex final shape occurs is depending upon the effects of these three sources.

Plastic strain distribution

As seen from Fig. 6(a), the resulting displacements of the loading step for two energy levels are very close, i.e. -2μm for low energy and -3μm for high energy, but the displacement after unloading for 3.57GW/cm^2 reaches -12μm while that of 4.95GW/cm^2 is only -6μm. This downward displacement reinforces the plastic deformation on the bottom side. Fig. 6(b) shows the time history of plastic strain in the lateral direction. It can be seen that plastic strain on the bottom side increases along the displacement while it is mainly determined by the period of the shock loading for the top side. For 4.95GW/cm^2, plastic strain on the top side is much larger than that of the bottom side, but the plastic strains on both sides are almost same for 3.57GW/cm^2. This difference makes the difficulty of upward bending for 3.57GW/cm^2 case, but favors upward bending for 4.95GW/cm^2. Hence, it is easier to induce convex bending with a high energy rather than a low one.

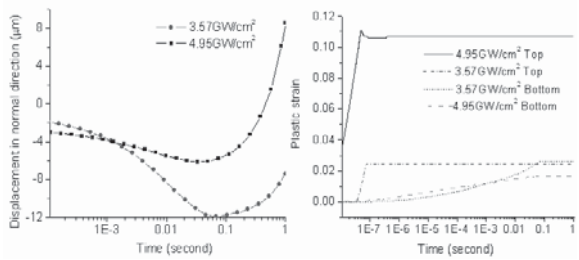

FIG. 6 TIME TRACE BY FEM SIMULATION: A) NORMAL DISPLACEMENT OF THE CENTER POINT ON THE BOTTOM SURFACE; B) PLASTIC STRAIN (ALONG SURFACE DIRECTION) OF THE CENTER POINT FOR BOTH SIDES OF SURFACE

Compressive stress distribution

From both experimental and simulation results, we found that both sides have compressive residual stresses for convex bending and one side is tensile and the other side is compressive for concave bending. Fig. 7(a) gives the time history of stress for the center point on the top surface. It indicates that the stress on the bottom is first tensile to balance the compressive stress of the top surface and then changes to compressive as the specimen bends upward for the 4.95GW/cm^2 laser intensity. For the case of 3.57GW/cm^2, the tensile residual stress occurs on the treated surface as the bending is reversed.

Fig. 7(b) shows the distribution of averaged stress within 30μm from the top right after the moment of unloading for two energy levels. This demonstrates that the range and magnitude of compressive stress induced by 4.95GW/cm^2 are much larger than those by 3.57GW/cm^2. The range of compressive stress for 4.95GW/cm^2 is around ±200μm while that of 3.57GW/cm^2 is only ±100μm. The effect of bending moment is relatively small compared with that of compressive stress since the bending angle is very small (~0.1°). Therefore, the induced compressive stress plays a dominant role in the bending after unloading. The wider of the compressive stress distribution, the harder of downward bending. Therefore, it is more difficulty to have convex shape happen for low energy than high energy in terms of compressive stress distribution. Wave propagation of the point 60μm away from the center on the top surface as shown in Fig. 7(c) gives some insight of the difference of compressive stress distribution for these two cases. From Fig. 7(c), we can see the pressure at that point for 4.95GW/cm^2 is twice and half times of that of 3.57GW/cm^2; that is, the effected area by 4.95GW/cm^2 is larger comparing to 3.57GW/cm^2 since shock wave can propagate much far for 4.95GW/cm^2. But in depth direction, shock wave propagation for both cases as shown in Fig. 7(d) is similar. The difference of wave propagation in depth and surface directions may be due to the material volume that can be compressed. For either case, there is little material which can be compressed in depth direction because the thickness is too thin. But for the surface direction, there is enough material for compressing.

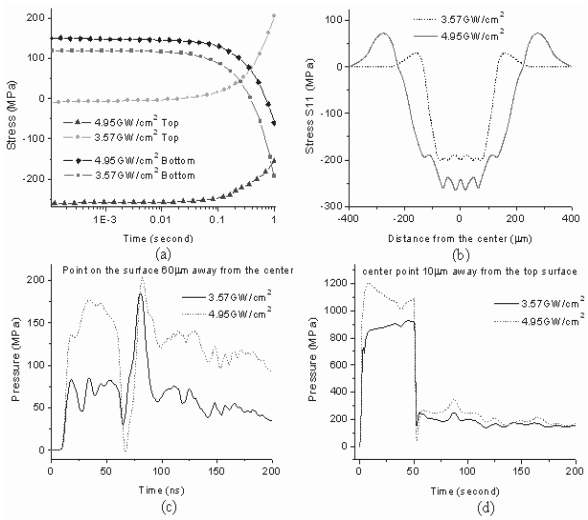

FIG. 7 STRESS AND WAVE PROPAGATION FROM FEM: A) TIME TRACE OF LATERAL STRESS OF THE CENTRAL POINTS ON BOTH SIDES OF SURFACE; B)SPATIAL DISTRIBUTION OF STRESS ON THE TOP SURFACE AT THE BEGINNING OF UNLOADING; C) WAVE PROPAGATION ALONG THE SURFACE DIRECTION ON THE TOP SURFACE; D) WAVE PROPAGATION IN DEPTH DIRECTION

The tension caused by compressive stress in 4.95GW/cm^2 case, which exerts bulging in the specimen, will restrain downward bending significantly compared to the 3.57GW/cm^2 case. That is why the downward bending of 4.95GW/cm^2 is smaller than that of 3.57GW/cm^2. After the combined effect of bending moment and compressive stress overcomes the downward effect caused by the inertia, the reverse bending follows. As discussed previously, the reverse magnitude is mostly determined by the induced compressive

stress and not the bending moment. Hence, the reverse magnitude of 4.95GW/cm^2 case is larger than that of 3.57GW/cm^2 case. For 4.95GW/cm^2 case, the compressive stress even overcomes the opposite bending moment and results in upward bending.

CONCLUSIONS

In this paper, micro-scale laser peen forming on copper samples of 100μm thickness with two levels of laser energy is investigated by using both experimental and numerical methods. The simulation model was verified by the experimental results measured by a profilometer and X-ray micro-diffraction. For 100μm samples, the bending mode is based upon applied laser energy. If 4.95GW/cm^2 laser intensity was applied, the bending is convex and the bending angle is around 0.14°. However, the bending is concave with the bending angle of 0.11° if the 3.57GW/cm^2 laser intensity was applied. This deformation phenomenon is explained by using the validated model in terms of the combined effects of three sources: impact (loading), induced compressive stress, and bending moment resulted by bending angle.

It was shown that the residual stress patterns are mainly determined by deformation mechanisms. For concave deformation, the bottom side is compressive while top is tensile. For convex bending, both sides are compressive. The maximum of compressive stress is -120MPa for 3.57GW/cm^2 and -160MPa for 100μm sample with a 4.95GW/cm^2 laser intensity. The effected area for both energy levels is around ±150μm, which is much larger than that of laser shock peening under the same conditions. In general, the extension of micro-scale laser shock peening to forming is valuable with respect to the residual stress distribution as well as the capability to deform the target at a micro-scale resolution.

REFERENCES

Chen, H, Yao, Y.L. and Kysar, J.W., 2004, "Spatially Resolved Characterization of Residual Stress Induced by Micro-scale Laser Shock Peening," *Journal of Manufacturing Science and Engineering, Transactions of the ASME*, Vol. 126, p226-236.

Clauer, A.H., and Holbrook, J.H., 1981, "Effects of Laser Induced Shock Waves on Metals," *Shock Waves and High Strain Phenomena in Metals—Concepts and Applications*, New York, Plenum, pp. 675-702.

Cullity, B.D., 1978, *Elements of X-ray Diffraction*, London, Addison-Wesley Publishing Company, Inc., 2nd edition, pp. 268-270.

Fabbro, R., Fournier, J., Ballard, P., Devaux, D., and Virmont, J., 1990, "Physical Study of Laser-produced Plasma in Confined Geometry," *J. Appl. Phys.*, Vol. 68 (2), pp. 775-784.

Hackel, Lloyd, Harris and Fritz, 2002, Contour Forming of Metals by Laser Peening, US Patent 6410884.

Vollertsen, F., 1994, "Mechanisms and Models for Laser Forming," *Laser Assisted Net Shape Engineering, Proceedings of the LANE'94*, B. Meisenbach eds., Vol. 1 pp. 345-360.

Zhou, M., Zhang, Y., and Cai, L., 2002, "Laser Shock Forming on Coated Metal Sheets Characterized by Ultrahigh-Strain-Rate Plastic Deformation," *Journal of Applied Physics*, Vol. 91, No. 8, p5501-5503.